Incremental Nonlinear Dynamic Inversion controller for a Variable Skew Quad Plane

De Ponti, T. M.L.; Smeur, E. J.J.; Remes, B. W.D.

DOI
10.1109/ICUAS57906.2023.10156289

Publication date
2023

Document Version
Final published version

Published in
2023 International Conference on Unmanned Aircraft Systems, ICUAS 2023

2023 International Conference on Unmanned Aircraft Systems (ICUAS)
June 6-9, 2023 | Lazarski University, Warsaw, Poland

2023 International Conference on Unmanned Aircraft Systems (ICUAS) | 979-8-3503-1037-5/23/$31.00 ©2023 IEEE | DOI: 10.1109/ICUAS57906.2023.10156289

Incremental Nonlinear Dynamic Inversion controller for a Variable Skew Quad Plane

T.M.L. De Ponti
Faculty of Aerospace Engineering
Control & Simulation
TuDelft
Delft, the Netherlands
t.m.l.deponti@tudelft.nl

E.J.J. Smeur
Faculty of Aerospace Engineering
Control & Simulation
TuDelft
Delft, Netherlands
E.J.J.Smeur@tudelft.nl

B.W.D. Remes
Faculty of Aerospace Engineering
Control & Simulation
TuDelft
Delft, Netherlands
B.D.W.Remes@tudelft.nl

***Abstract*—This paper presents the design of an Incremental Nonlinear Dynamic Inversion (INDI) controller for the novel, patent pending (NL 2031701) platform Variable Skew Quad Plane (VSQP). Part of the identified challenges is the development of a model for the actuator effectiveness and lift especially as a function of skew, the newly added degree of freedom. The models and assumptions are verified through static and dynamic wind tunnel tests at the Open Jet Facility (OJF) of TU Delft. Transition tests have been successfully performed thanks to an automatic skew controller derived from the proposed models and aimed to maximize control authority.**

***Index Terms*—INDI, Variable Skew Quad Plane, UAV modelling, transition.**

I. Introduction

Unmanned Air Vehicles (UAVs) have grown in popularity thanks to their ability to perform tasks autonomously without requiring the intervention of an operator. In addition, the ease of operation achieved by hybrid UAVs in vertical as well as cruising phases offers a cheaper and more straightforward solution compared to user based vehicle operation. Hybrid UAVs embed in their design VTOL capabilities typical of multicopters but are also able to harness the efficiency of a wing in cruise thanks to a transitioning procedure. This transition can simply involve a change in attitude and control or require a mutation in the fundamental geometry of the drone.

Applications such as high-rise package delivery, off-shore missions and landings on moving platforms require good wind rejection capabilities. Therefore, there is the need for a platform able to operate in gusty environments in an autonomous and efficient way using only a very limited input from an operator. The design under development is best described as a Variable Skew Quad Plane (VSQP) and to the best knowledge of the author it is a first in its category.

II. Background on the Platform

Wijngaarden and Remes[1] first describe the functioning of the VSQP. In hover mode, the drone operates as a quad-rotor and attitude is controlled through differential thrust. In forward flight mode the drone operates as a plane and uses aerodynamic surfaces to achieve attitude control. Similarly to a typical quad-plane, the drone achieves forward speed

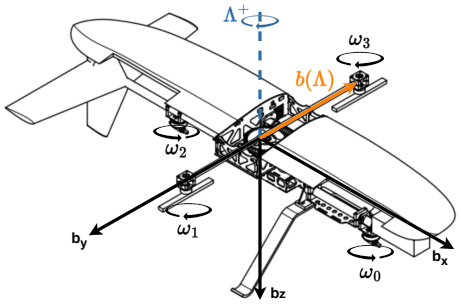

Fig. 1. Variable Skew Quad Plane (VSQP) with skew angle Λ set to 0°

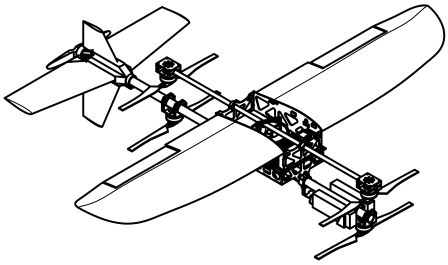

Fig. 2. VSQP with skew angle Λ set to 90°[1].

thanks to a push propeller placed at the tail. In contrast to a quad-plane, the proposed design does not have a fixed wing configuration, but rather implements the rotating concept applied in a Oblique Flying Wing (OFW)[2]. A central rotating structure is used to deploy the wing as the lateral rotors are folded in the fuselage. This approach is expected to greatly increase cruise efficiency thanks to the combination of the wings lift generation benefits as well as drag reduction from the retraction of the unused rotors. Moreover, it is expected that in hover mode, by housing the wing on top of the fuselage, the area upon which wind gusts can act is reduced, in turn increasing control authority. Figure 1 and Figure 2 show the VSQP in respectively the hover and forward flight mode. These are drawings from a preliminary CAD assembly of the VSQP and lack the fuselage components which are

under development.

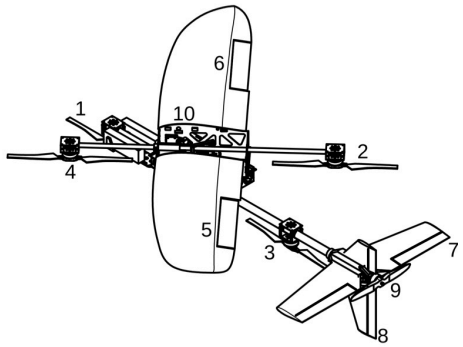

Fig. 3. Actuator schematic of the VSQP[1].

TABLE I
LIST OF ACTUATORS FOR THE OBLIQUE WING-QUAD PLANE DRONE[1].

Actuator number	Actuator name	Rotating
1	Front Motor	
2	Right Motor	✓
3	Back Motor	
4	Left Motor	✓
5	Left Aileron	✓
6	Right Aileron	✓
7	Elevator	
8	Rudder	
9	Push Motor	
10	Wing Rotation Servo	

In order to achieve guidance and stabilization the VSQP uses a total of 10 actuators which are reported in Table III. Figure 3 shows a graphical representation of the placement of the actuators on the VSQP. The right column of the table shows whether the actuator is rotating with skew angle.

III. MODEL OF VSQP

The VSQP is stabilized and guided through Incremental Nonlinear Dynamic Inversion control (INDI). INDI has been described since the late 1990s to be a less model dependent and more robust solution than other more conventional control methods [3]. The idea behind INDI is to replace part of the dynamic model of the platform with data retrieved online by sensor readings. The development of accurate models of Micro Air vehicles (MAV) using flight data can indeed require expensive resources and is limited by the small sensors which can be carried by a MAV [4]. In INDI, given that actuator feedback is available, modelling is restricted to only the drafting of the effectiveness matrix which contains the effectiveness values of the actuators. The VSQP is overactuated in both stabilization and guidance, therefore a Weighted Least Squares (WLS) routine, as described by Smeur and Höppener [5] and Karssies and de Wagter [6], is performed.

In order to apply the INDI control law, a precise definition of the control effectiveness matrix over the flight envelope is required. Actuators generate angular accelerations by exerting a moment on the drone. Therefore, an expression for the total exerted moment from the actuators M_c is needed:

$$M_c\left(\omega,\delta,\Lambda,v\right)=M_{c_m}\left(\omega,\Lambda,v\right)+M_{c_{as}}\left(\delta,\Lambda,v\right), \quad (1)$$

where ω is the vector containing the rotational speed of the motors, δ is the vector containing the deflection of the aerodynamic surfaces, Λ is the skew angle, v is the airspeed, M_{c_m} is the moment exerted by the motors and $M_{c_{as}}$ is the moment exerted by the aerodynamic surfaces.

A. Control Moment due to the Motors

Blade Element Momentum Theory (BEMT) predicts that the output thrust changes quadratically with the rotational rate [7]. This conclusion is confirmed by data registered from a motor bench test of the motor-prop combination used in the VSQP [8]. A quadratic function fit of the rotational speed approximates the thrust with an Root Mean Square Error (RMSE) of $9.34\text{e}{-2}$ N and maximum error of $2.49\text{e}{-1}$ N over a registered range of 16 N. Similarly, the exerted torque is approximated with an RMSE of $1.40\text{e}{-3}$ Nm and maximum error of $3.40\text{e}{-3}$ Nm over a registered range of 0.26 Nm. It follows that the thrust T_i and torque Q_i vector in space for any given motor i can be approximated as:

$$T_i\left(\omega_i\right)=\begin{bmatrix} n_x & n_y & n_z \end{bmatrix}^{\mathsf{T}}\left(k_{t_i}\omega_i^2\right), \quad (2)$$

$$Q_i\left(\omega_i\right)=\begin{bmatrix} n_x & n_y & n_z \end{bmatrix}^{\mathsf{T}}\left(k_{q_i}\omega_i^2\right), \quad (3)$$

where k_{x_x} is the quadratic coefficient of the thrust/torque curve and $\vec{n}$ is the unit vector that defines the direction in space of the thrust vector of motor i. Now that the thrust force and reactionary torque have been defined as a function of rpm, it is possible to derive an expression for the exerted moment from any given motor i.

$$M_{\mathrm{m_i}}\left(\omega_i,\Lambda\right)=b_i\left(\Lambda\right)\times T_i\ \left(\omega_i\right)+Q_i\left(\omega_i\right), \quad (4)$$

where $M_{\mathrm{m_i}}\left(\omega,\Lambda\right)$ is the moment exerted by motor i and $b_i\left(\Lambda\right)$ is the moment arm vector of motor i. Now, in order to express $b_i\left(\Lambda\right)$ in more detail, the following definition for the vector d_{cg} connecting the center of gravity to the rotation point is introduced:

$$d_{cg}=\begin{bmatrix} x_{\mathrm{rp}}-x_{\mathrm{cg}} & y_{\mathrm{rp}}-y_{\mathrm{cg}} & z_{\mathrm{rp}}-z_{\mathrm{cg}}. \end{bmatrix}^{\mathsf{T}}. \quad (5)$$

Furthermore, the vector d_{rp} connecting the rotation point to a given motor i is defined as:

$$d_{rp}=\begin{bmatrix} x_{\mathrm{mot_i}}-x_{\mathrm{rp}} \\ y_{\mathrm{mot_i}}-y_{\mathrm{rp}} \\ z_{\mathrm{mot_i}}-z_{\mathrm{rp}} \end{bmatrix}=\begin{bmatrix} j_{0_x} \\ j_{0_y} \\ j_{0_z} \end{bmatrix}b, \quad (6)$$

where $\vec{x_{cg}}$ is the position of the Center of Gravity (C.G.) in space, $\vec{x_{rp}}$ is the position of the Rotation Point in space, $\vec{x_{mot_i}}$ is the position of Motor i in space, $\vec{j_0}$ is the unit vector of the moment arm and b is the length of the moment arm. It follows then that the moment arm vector at any skew angle in the body reference frame can be described by applying a rotation around the z axis by the additive inverse of the skew

angle.

$$b(\Lambda) = \begin{bmatrix} b_x \\ b_y \\ b_z \end{bmatrix} = R_z(-\Lambda)\ j_0\ b\ + s_{\text{cg}} = \begin{bmatrix} \cos(\Lambda) & -\sin(\Lambda) & 0 \\ \sin(\Lambda) & \cos(\Lambda) & 0 \\ 0 & 0 & 1 \end{bmatrix} \begin{bmatrix} j_{0_x} \\ j_{0_y} \\ j_{0_z} \end{bmatrix} b + \begin{bmatrix} d_{\text{cg}_x} \\ d_{\text{cg}_y} \\ d_{\text{cg}_z} \end{bmatrix} = j\ b + d_{cg}. \tag{7}$$

Equation (4) can be evaluated for each of the four quad motors. It must be realized that the longitudinal motors do not change position as the wing is rotated, thus their skew angle is always $0°$. The VSQP was designed so to have the C.G. coincident with the rotation point thus leading to negligible s_{cg}.

$$M_{c_m} = \begin{bmatrix} 0 & -b_2\, k_{t_2}\, \cos(\Lambda) & 0 & b_4\, k_{t_4}\, \cos(\Lambda) \\ b_1\, k_{t_1} & -b_2\, k_{t_2}\, \sin(\Lambda) & -b_3\, k_{t_3} & b_4\, k_{t_4}\, \sin(\Lambda) \\ k_{q_1} & -k_{q_2} & k_{q_3} & -k_{q_4} \end{bmatrix} \vec{\omega}^2 \tag{8}$$

Equation 8 highlights that as the wing is deployed, the control moment exerted by the side motors shifts from the roll axis to the pitch axis. The longitudinal motors instead only act around the pitch axis.

B. Control Moment due to the Aerodynamic Surfaces

Forces and moments generated by the aerodynamic surfaces are modeled using simple lifting theory. Lift is assumed to be mainly generated by the chordwise component v_C of the airspeed vector v.

$$v_C = \sin(\Lambda) v \tag{9}$$

The Lift generated by a aerodynamic surface i is then:

$$L_i = C_{L_i}(\alpha) \frac{1}{2}\, \rho\, S\, \sin(\Lambda)^2\, v^2, \tag{10}$$

where L_i is the lift generated by A.S. i, C_{L_i} is the lift coefficient of A.S. i, ρ is the air density and S is the surface area of A.S. i.

Now, further assuming that the angle of attack of an aerodynamic surface is equal to its deflection angle δ_{as_i} and that the lift coefficient changes linearly with such angle, it is possible to develop (10) into:

$$L_i = k_{as_i}\, \delta_{as_i} \frac{1}{2}\, \rho\, S\, \sin(\Lambda)^2\, v^2 \tag{11}$$

Where k_{as_i} is a constant coefficient that can be estimated from test flight or wind tunnel experiments. It follows then that the exerted moment of a given aerodynamic surface i is:

$$M_{\text{as}_\text{i}}(\delta, \Lambda, v) = b_i(\Lambda) \times L_i\ (\delta, \Lambda, v) \tag{12}$$

The moment arm $b_i(\Lambda)$ is defined as in (7). The aerodynamic surfaces on the tail do not change position as the wing is deployed. Therefore their Lift and moment arm is calculated at a constant skew of $0°$. Evaluating (12) for each of the four aerodynamic surfaces leads to :

$$M_{c_{as}} = \begin{bmatrix} b_{\text{al}}\, k_{\text{al}}\, v^2 \sin(\Lambda)^3 & -b_{\text{al}}\, k_{\text{ar}}\, v^2 \sin(\Lambda)^3 & 0 & 0 \\ -b_{\text{al}}\, k_{\text{al}}\, v^2 \left(\cos(\Lambda) - \cos(\Lambda)^3\right) & b_{\text{al}}\, k_{\text{ar}}\, v^2 \left(\cos(\Lambda) - \cos(\Lambda)^3\right) & -b_{\text{el}}\, k_{\text{el}}\, v^2 & 0 \\ 0 & 0 & 0 & -b_{\text{ru}}\, k_{\text{ru}}\, v^2 \end{bmatrix} \begin{bmatrix} \delta_{\text{al}} \\ \delta_{\text{ar}} \\ \delta_{\text{el}} \\ \delta_{\text{ru}} \end{bmatrix} \tag{13}$$

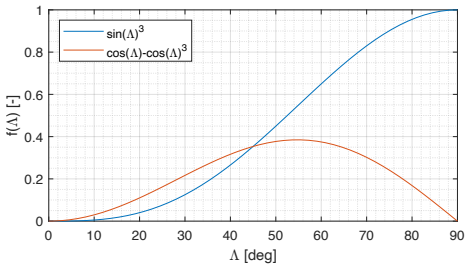

Fig. 4. Evolution of control moment model of the ailerons with skew ($\Lambda = 0°$ Quad mode, $\Lambda = 90°$ Flight Forward mode).

Figure 4 reports the evolution of the identified trigonometric relationships of Equation 13 with skew. Figure 4 highlights that as the wing is skewed, the ailerons are expected to exert more moment around the roll axis achieving peak effectiveness in forward mode. On the contrary, the maximum moment exerted by the ailerons around the y axis is not achieved at either skew extremes but rather at $54.7°$. This is the result of the pitch moment arm shortening with skew while the chordwise component of airspeed increases. The moment exerted by the elevator and by the rudder instead changes only with airspeed and is not expected to be affected by skew.

IV. Lift Model

A precise lift model has the benefit of providing insight into how guidance and transition should be performed by the VSQP. In the guidance outer loop an estimation of $\frac{\partial L}{\partial \theta}$ is used to determine which change in pitch angle is needed to track the linear acceleration reference and provides important envelope limits as stall and lift-off conditions. These insights can then be used to schedule the pitch, airspeed and skew profile to safely perform the transition.

The first assumption in the drafting of the lift model is level flight. This allows to approximate the angle of attack with the pitch angle. This assumption simplifies the drafting of the lift model because pitch can be measured by the basic sensors onboard of the VSQP while an extra alpha vane would have

to be added to the platform to precisely measure the angle of attack.

Similarly to the aerodynamic surfaces, it is assumed that most of the lift is generated by the chordwise component of airspeed, leading to an initial lift model similar to (10). However, at the current development stage of the VSQP, no fuselage has been designed yet. Therefore, the wings at 0° skew have a non negligible cross-section which is swept by the airflow. Consequently, it is expected that the wings are able to generate a limited amount of lift also in quad mode. Therefore, the relationship between lift and skew can be modeled as a linear function of $sin(\Lambda)^2$ with a constant offset k_1. The lift coefficient, if the wing is not stalled, is expected to change linearly with θ and to have an offset k_2 in the case that lift is generated also at 0° pitch angle. With these insights in mind, it is possible to draft a lift model of the VSQP:

$$\begin{aligned} L(\theta,\Lambda,v) &= \frac{1}{2}\rho S v^2[m_1\sin(\Lambda)^2 + k_1][m_2\theta + k_2] \\ &= \frac{1}{2}\rho S v^2[m_1 m_2\theta\sin(\Lambda)^2 + m_1 k_2\sin(\Lambda)^2 + k_1 m_2\theta + k_1 k_2] \\ &= \frac{1}{2}\rho S v^2[\lambda_1\theta\sin(\Lambda)^2 + \lambda_2\sin(\Lambda)^2 + \lambda_3\theta + \lambda_4]. \end{aligned} \tag{14}$$

Equation 14 can then be differentiated with respect to θ in order to provide an estimation of $\frac{\partial L}{\partial\theta}(\Lambda, v)$ to be used in the guidance of the VSQP:

$$\frac{\partial L}{\partial\theta}(\Lambda, v) = \frac{1}{2}\rho S v^2[\lambda_1\sin(\Lambda)^2 + \lambda_3]. \tag{15}$$

The coefficients $[\lambda_1, \lambda_2, \lambda_3, \lambda_4]$ of (14) can be estimated by performing a least squares estimation on flight or wind tunnel data having as variables $[\theta\sin(\Lambda)^2,\ \sin(\Lambda)^2, \theta, 1]$.

V. Verification

Wind tunnel data and post processing scripts can be found in [8] together with Appendix A containing the graphical representation of the conclusions about the verification of the exerted moment model of the aerodynamic surfaces and Appendix B cointaining a summary of the test setup.

In order to verify the developed models of $M_c(\omega, \delta, \Lambda, v)$ and $L(\theta, \Lambda, v)$, and estimate the unknown coefficients, static and dynamic tests of the VSQP were designed and performed at the Open Jet Facility (OJF) at the aerodynamics department of Faculty of Aerospace Engineering of TuDelft, a large wind tunnel with an open test section of 2.85 m by 2.85 m.

The OJF External Balance B8604 is used to provide force and moment readings. The balance is mounted on a turn table which can rotate the full assembly by 360°. A test using only the pole structure and attachments was used to remove their contribution to the balance readings from the dataset. Moreover, by knowing the dimensions of the pole expressed as a vector l_p it is possible to shift the force and moment readings at the balance (F_b and M_b) to the C.G. of VSQP ($F_{C.G.}$ and $M_{C.G.}$):

$$F_{C.G.} = F_b \tag{16}$$

$$M_{C.G.} = M_b + l_p \times F_b \tag{17}$$

A. Motors

A combination of dynamic and static tests were designed to verify the derived model for Equation 8. In the dynamic tests, while the VSQP was airborne, a series of doublet signals were sent to the four hovering motors. During the activation time of the doublet signal, all other actuators received a constant command. This procedure was repeated for all four quad motors and at different skew angles. The angular rates, as recorded by the Inertial Measurement Unit (IMU), are differentiated to obtain an angular acceleration signal which is then compared to the command sent to the actuators. A first order dynamics model is used to estimate the state of the actuator. A low pass filter is applied to both the reconstructed state signal and to the angular acceleration signal to remove noise and maintain sync. A linear least squares is then used to estimate the effectiveness values of the motors.

Figure 5 shows the estimated roll and pitch effectiveness values of the quad motors at different skew angles up to 60° in hovering condition. It was not possible to obtain data points at higher skew angles as the roll effectiveness becomes too low to maintain stable flight. Figure 5 highlights that the roll effectiveness of the longitudinal motors (motor front and motor back) is constant with skew and close to zero. Figure 5 also shows that the pitch effectiveness of the longitudinal motors is constant with skew but non-zero as predicted by (8).

As for the side motors, Figure 5 shows that roll effectiveness decreases as skew is increased. In contrast, the pitch effectiveness increases with skew and converges to the values estimated for the longitudinal motors. These conclusions are in line with the predictions from (8). A data fit curve using the trigonometric relationships of the developed model results in a small RMSE of $1.39\text{e}0$ and $2.83\text{e}{-1}$ $[\frac{rad}{s^2 pprz}]$[1] for roll and pitch effectiveness of the side motors. The small RMSE suggests that the developed model of (8) can be used to accurately describe the control capabilities of the quad motors.

A further static test with a motor test-bench was set up to understand the relationship between thrust and airspeed. In (2) it was indeed assumed that the thrust is simply dependent on ω but a series of works in the literature have highlighted increased thrust of propellers in crossflow [10, 11, 12]. The test though has concluded that in the expected envelope of utilization of the motors the maximum increase in thrust is only about 6.7%. Furthermore, such increase in thrust is dependent on airspeed which changes at a much slower rate compared to the actuator dynamics. Therefore, due to the incremental nature of INDI's control law, it is expected that the controller will compensate for such modelling inaccuracy.

[1] $pprz$ is the basic command unit of Paparazzi UAV [9], the used autopilot firmware on the VSQP.

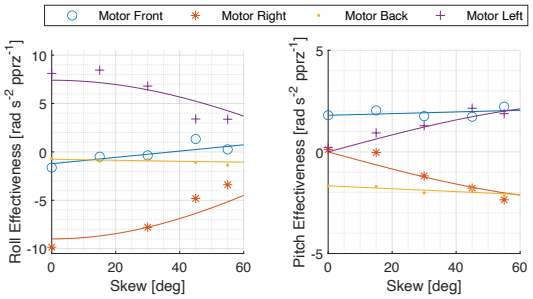

Fig. 5. Evolution of roll and pitch effectiveness of quad motors with skew at $v = 0$ m/s ($\Lambda = 0°$ Quad mode, $\Lambda = 90°$ Flight Forward mode).

B. Aerodynamic Surfaces

Data from the static test at $0°$ pitch and $60°$ skew angle are used to verify the assumptions utilized in the developed model. The specific skew of $60°$ was chosen because this is the state in which the ailerons are predicted to be effective in both roll and pitch, but all conclusions also hold for other skew angles. Pulse Width Modulation (PWM) is used as an indication of the state of the aerodynamic surfaces as these are deflected by electric servos.

A linear function of PWM is able to approximate the registered exerted moments from the aerodynamic surfaces with a small average RMSE of $2.90\text{e}{-2}$ Nm, $1.51\text{e}{-1}$ Nm and $1.65\text{e}{-2}$ Nm for the left aileron, right aileron, elevator and rudder respectively. These insights verify the first adopted assumption of linearity between state of the aerodynamic surfaces and respective exerted moments.

Similarly, data at $0°$ pitch and $60°$ skew angle show that a quadratic function of airspeed is able to approximate the registered exerted moments with a small average RMSE of $4.38\text{e}{-2}$ Nm, $4.12\text{e}{-2}$ Nm, $1.51\text{e}{-10}$ Nm and $1.61\text{e}{-2}$ Nm for aileron left, aileron right, elevator and rudder respectively. These conclusions verify that the exerted moment from the aerodynamic surfaces can be accurately modeled quadratically with airspeed.

Data from the static test at $0°$ pitch and 9 m/s airspeed are used to verify that the developed moment-skew relation from (13) is an accurate representation of the capabilities of the aerodynamic surfaces. This specific airspeed is chosen because the drone is expected to be in transition at this stage, thus being in the process of deploying the wing.

Starting from the roll moment exerted by the ailerons, a function $k\ \sin(\Lambda)^3$ results in a fit curve with a small average RMSE of $2.82\text{e}{-2}$ Nm and $4.45\text{e}{-2}$ Nm for the left and right aileron respectively. The small approximation errors are an indication that the developed trigonometric relationship between skew and exerted roll moment models correctly the roll capabilities of the ailerons.

As for the pitch moment exerted by the ailerons, the data shows that it tends to zero at the two skew extremes of $0°$ and $90°$ and is maximum in between the skew angles of $50°$ and $60°$. As predicted by (13) a function $k\ (cos(\Lambda) - cos(\Lambda)^3)$ results in a fit of the data points with a contained average RMSE across the dataset of $1.65\text{e}{-2}$ Nm and $3.23\text{e}{-2}$ Nm for the left and right aileron respectively. This is an indication that the identified trigonometric relationship between skew and exerted pitch moment well models also the pitch capabilities of the ailerons.

As for the tail surfaces, in (13) it was predicted that skew does not affect the control capabilities of the elevator and rudder. The data indeed show that for any given actuator state the exerted moment is constant and can be approximated by a linear function with negligible slope.

C. Lift Model

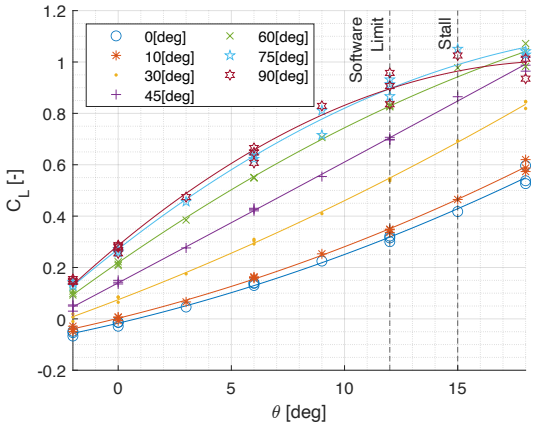

Fig. 6. C_L curve at different airspeed

Equation 14 presented a modelling structure for the lift generated by the wing at different θ, Λ and airspeed. Level flight is assumed so to approximate α with θ. The model was derived by simple lift theory and it is assumed that most of the lift is generated by the chordwise component of airspeed. Furthermore, it is assumed that away from the stall region, lift changes linearly with pitch angle.

A static test with variable pitch provided by the turn table is used to verify the lift model. Figure 6 shows the evolution of the lift coefficient with pitch angle at different skew settings. The lift coefficient was computed according to (18).

$$C_L = \frac{L\,(\theta, \Lambda, v)}{\frac{1}{2}\rho S v^2} \tag{18}$$

Figure 6 shows that at $90°$ skew, C_L starts to drop past $12°$ pitch indicating the beginning of stall. Similar conclusions are achieved through a simulation in XFLR5 for the airfoil MH32 of the wing. A 20% lower softer limit ($12°$) than the identified stall point is used to assure that the VSQP does not suddenly stall. Figure 6 shows that under the software limit, C_L changes linearly with pitch for all skew angles. Therefore, the assumption of linearity between lift and pitch is verified.

Furthermore, Figure 6 shows that the difference between C_L at all pitch angles tends to zero at the skew extremes of $0°$ and $90°$ and is largest around $45°$. This trend matches the characteristics of the trigonometric function $\sin(\Lambda)^2$ whose derivative is maximized at $45°$ and then rapidly tends to zero

close to $0°$ and $90°$. Moreover, Figure 6 also shows that at $0°$ skew the wing generates lift, justifying the need to introduce and offset in the lift-skew modelling.

Performing a least square approximation of the data points from the static test using the modelling structure of (14) leads to a RMSE across the dataset of only $4.00\text{e}{-1}$ N indicating that the model truthfully represents the lift capabilities of the wing at different θ, Λ and airspeed.

VI. Automatic Skew Controller

The models presented in section III allow to precisely estimate the lift and exerted control moment at any given airspeed and skew angle. Therefore, an optimization problem can be defined to evaluate the skew angle that maximizes control authority at any given airspeed.

The optimization problem consists of a linear programming problem for each of the three stabilization axes. The variables for these linear programming problems are the actuator states. The objective function per axis is defined by the corresponding row in the matrix that defines the total exerted control moment model as in (1).

Each actuator state is constrained to not exceed its minimum and maximum saturation limits. Furthermore, it is expected that the found solutions are maneuvers that can be performed without losing control of other axes. Therefore, the found solution should result in zero moment around the remaining stabilization axes. This is ensured by enforcing the remaining rows of (1) to be zero.

The sum of thrust as calculated in (2) and lift (14) is set to be higher than or equal to the weight of the drone. A summary of the setup of the linear optimization problem for a sample calculation of the maximum exerted roll moment can be found in Appendix C at [8].

Now, the results of the optimization problems carried out at each skew and airspeed combination are three surfaces $(S_\phi, S_\theta, S_\psi)$ indicating the maximum roll, pitch and yaw moment that the actuators can achieve. Therefore, these surfaces indicate which skew angle maximizes the exerted control moment around a specific axis at any given airspeed.

A fourth surface is further introduced to represent the total thrust required at each skew-airspeed combination. This is equal to the amount of thrust that the quad motors have to deliver to maintain altitude and the thrust required from the pusher motor to maintain a specific airspeed. The quad thrust is approximated to be the force needed on top of the estimated lift to match the weight of the drone. The pusher thrust has been modeled linearly with v^2.

$$T_{\text{tot}}(\Lambda, v) = T_{\text{quad}} + T_{\text{push}} = \max(\text{m}g - L(\theta, \Lambda, v), 0) + av^2 \tag{19}$$

Now, since the goal is to find the skew angle that minimizes the required thrust level and consequently the energy consumption, the actual surface S_T that will be used for further conclusions is the inverse of T_{tot}.

$$S_T(\Lambda, v) = \frac{1}{T_{\text{tot}}(\Lambda, v)} \tag{20}$$

In order to compare the surfaces and draw conclusions, each surface is normalized with its maximum as shown in (21).

$$S_{i_{\text{norm}}} = \frac{S_i}{\max(||S_i||)} \tag{21}$$

Finally, the surfaces are combined into a general surface S_{tot} through the use of a vector γ of weight coefficients.

$$S_{\text{tot}} = \gamma * \begin{bmatrix} S_\phi & S_\theta & S_\psi & S_T \end{bmatrix}^{\mathsf{T}} \tag{22}$$

The weights are chosen to establish a desired hierarchy between the transition objectives.

The primary goal during transition is to change geometry from quad to fixed wing, to maximize energy efficiency. Therefore, the highest weight of 4 is assigned to S_T. Both θ and ϕ determine the direction of the quad thrust. Therefore, failing to track the reference signals of θ and ϕ can lead to loss in altitude. The CAD model of the VSQP indicates that I_{xx} is 5.79% of I_{yy}. This is because most of the mass is placed along the longitudinal line of the drone. Therefore, maximizing pitch control should have a higher priority, as roll deviations can be corrected less expensively. It follows that S_θ is assigned a higher weight than S_ϕ, three and two respectively. Finally the lowest weight of 1 is then assigned to S_ψ.

Evaluating (22) with the described weights leads to S_{tot} as shown in the contour plot in Figure 7. Now, a straightforward way to schedule Λ with airspeed would be to evaluate which skew setting maximizes S_{tot} at each considered airspeed. This approach results in the red line in Figure 7. The problem with this approach is that moving from a maximum point to the other can involve first sweeping through a dipping region of the surface or in other words a lower control authority state of the drone. A better solution would be to command

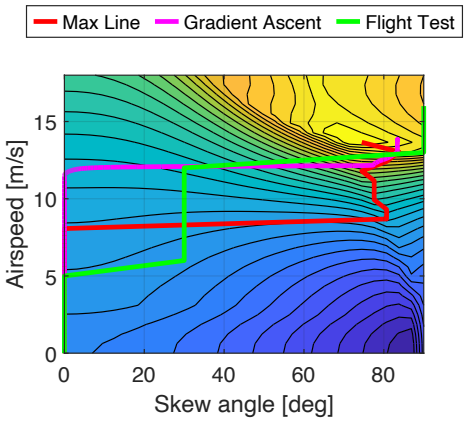

Fig. 7. Contour plot of S_{tot} and skew scheduling strategies.

skew changes which only increase the control authority of the drone even at the cost of not reaching the maximum as fast. In other words, a modified gradient ascent algorithm can be used to determine a path which changes skew only when

the partial derivative $\frac{\partial S_{tot}}{\partial \Lambda}$ is positive. The definition of a general gradient ascent method is:

$$X_{n+1} = X_n + \alpha \, \nabla S_{\text{tot}}\left(X_n\right), \tag{23}$$

where X_n is a vector containing $[\Lambda, v]$ at step n and α is the learning rate. The gradient is calculated as:

$$\nabla S_{\text{tot}}\left(X_n\right) = \left[\begin{array}{c} \frac{\partial}{\partial \Lambda} S_{\text{tot}}\left(X\right) \\ \frac{\partial}{\partial v} S_{\text{tot}}\left(X\right) \end{array} \right] | X = X_n. \tag{24}$$

In the classical gradient ascent algorithm α is chosen to be a single constant number. On one hand, this results in path changes which are perpendicular to the isometric lines, resulting in the steepest ascent of the curve. On the other hand, it can be argued that such behavior is not optimal as airspeed is the output of the guidance module rather than the skew controller. Making the example of the VSQP following a ship at sea, the wanted airspeed is determined by the speed of the moving target. The skew controller should then command a Λ which maximizes control at that specific target airspeed. In a nutshell, two learning rates $[\alpha_\Lambda, \alpha_v]$ can be defined, one for each of the calculated partial derivatives of (24). It is then possible to assure an ascent of the curve which encourages changes in Λ by choosing $\alpha_v << \alpha_\Lambda$.

The result of this modified gradient ascent is shown in Figure 7. The result indicates that before $12\ \mathrm{m/s}$ changing skew angle is not beneficial towards ascending the surface. After $12\ \mathrm{m/s}$ the preferred skew is $90°$ which indicates that all other settings in between are deemed to have less control authority.

This conclusion is also confirmed by multiple test flights performed at the OJF wind tunnel as explained in more detail in section VII. Figure 7 shows that the skew scheduling used in the flight tests well resembles the result of the gradient ascent method. In the flight test, the best configuration is found to be a rapid increase in skew at $12\ \mathrm{m/s}$. Differently from the gradient ascent results though, at $5\ \mathrm{m/s}$ the preferred skew is $30°$. This is the result of an observed reduced stability of the VSQP at $0°$ skew in the airspeed region of $5 - 8\ \mathrm{m/s}$. In this state the drone experiences a heavy pitch up moment which saturates the longitudinal motors. This is thought to be the result of unmodelled aerodynamic interactions in between the wing, the horizontal surface and the back motor, but more scientific insight is needed to further support this conclusion.

VII. Validation

The developed controller is validated by means of free flight in the OJF wind tunnel. The drone was commanded to maintain its position in space autonomously as wind speed was varied.

Figure 8 reports data from a transition test. First, the OJF is activated and set to $18\ \mathrm{m/s}$. As airspeed increases, the skew angle controller commands higher and higher skew setpoint until forward flight mode is reached. Together with airspeed also the effectiveness of changing pitch to control linear vertical accelerations increases as predicted by the lift model. Therefore, the outer loop WLS routine evaluates that increasing the pitch angle and reducing the thrust from the quad results in a lower cost function. As a consequence, with the build up of airspeed also pitch increases and the quad motors are gradually turned off. Transition occurs with a remarkable tracking of the target altitude of $3\ \mathrm{m}$. The wind speed is maintained constant at $18\ \mathrm{m/s}$ for $20\ \mathrm{s}$ with the VSQP maintaining target position in space in flight forward mode. Subsequently, the airspeed is gradually reduced back to $0\ \mathrm{m/s}$. As soon as the controller senses a decrease in airspeed, maximum pitch is commanded and the quad motors are activated again. With the progressive reduction of airspeed, skew is commanded to return to zero and the VSQP completes the transition completely reliant on Quad thrust for attitude control. Figure 8 shows that throughout transition, the reference signal for pitch is closely tracked indicating a correct stabilization of the platform.

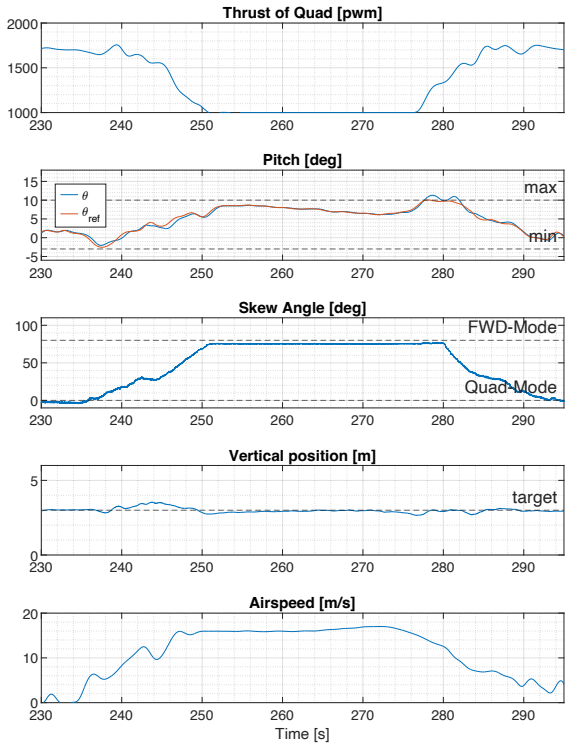

Fig. 8. Transition data

The transition was repeated successfully multiple times validating the controller for use in the controlled environment of the wind tunnel. Further research has to be conducted to also validate the controller in an outdoor turbulent gusty environment.

VIII. Conclusion

This paper has presented the derivation, verification and validation of an INDI controller which is able to stabilize the VSQP in all of its configurations.

The main research focus is the development of a model of the control effectiveness and a model of the lifting properties of the wing at any given state of the drone. These models are used by the autopilot to correctly calculate the necessary

control allocation to achieve stabilization and guidance. The static and dynamic tests verify the proposed model of (8),, (13) and (14) in each of their adopted assumptions. Therefore, the proposed models are concluded to be a truthful representation of the control capabilities of the aerodynamic surfaces and lifting properties of the wing. Therefore, these models have been used in the design of a INDI controller for the VSQP which allowed for multiple successful transitions.

In a nutshell, the models can be based on a few simple but powerful assumptions:

- Control effectiveness changes linearly with actuator state for all actuators.
- Control effectiveness changes quadratically with airspeed for the aerodynamic surfaces.
- Aerodynamic forces generated by the control surfaces and by the wing are mostly dependent on the chordwise component of airspeed which can be expressed in terms of the skew angle.
- The moment arm of the rotating actuators which affects their effectiveness is modeled as a vector rotating around the C.G. by an angle equal to the skew.

A. Future work

Future work will focus on transitions also outdoor so to validate the developed controller also in gusty turbulent environments. Moreover, more research should be conducted to understand the interaction between the motors and the lifting surfaces. Flow indicators placed at the horizontal tail have suggested that at low airspeed the back motor generates a negative angle of attack which can lead to negative lift. Initial analysis shows that this might contribute to the generation of a pitch up moment. Tests at different combinations of quad-motor and pusher motor setting should be performed to develop further scientific insights on the phenomenon. With such knowledge better design choices can be developed for the tail-back motor assembly and its control effectiveness modelling. Finally, it must be evaluated if the increased precision of the effectiveness model is also reflected by an increase in control performance or if it only adds complexity to the controller.

REFERENCES

[1] D. van Wijngaarden and B.D.W. Remes. "INDI Control for the oblique wing-quad plane drone". In: *13^{th} IMAV Conference*. Paper no. IMAV2022-14. Delft, the Netherlands, Sept. 2022.

[2] T. Mcmurtry, A. Sim, and W. Andrews. "AD-1 oblique wing aircraft program". In: *1st Flight Test Conference*. 1981.

[3] B. Bacon and A. Ostroff. "Reconfigurable flight control using nonlinear dynamic inversion with a special accelerometer implementation". In: *Guidance, Navigation, and Control Conference and Exhibit*. AIAA, Aug. 2000. DOI: 10.2514/6.2000-4565.

[4] E.J.J. Smeur, Q. Chu, and G.C.H.E. de Croon. "Adaptive Incremental Nonlinear Dynamic Inversion for Attitude Control of Micro Air Vehicles". In: *Journal of Guidance, Control and Dynamics* 39 (2016). DOI: 10.2514/1.g001490.

[5] E. J. J. Smeur and C. Höppener D. andde Wagter. "Prioritized Control Allocation for Quadrotors Subject to Saturation". In: *IMAV Conference and Flight Competition 2017* (2017).

[6] H.J. Karssies and C. de Wagter. "Extended incremental non-linear control allocation (XINCA) for quadplanes". In: *International Journal of Micro Air Vehicles* 14 (Jan. 2022). DOI: 10.1177/17568293211070825.

[7] R. MacNeill and D. Verstraete. "Blade element momentum theory extended to model low Reynolds number propeller performance". In: *The Aeronautical Journal* 121.1240 (2017). DOI: 10.1017/aer.2017.32.

[8] T.M.L. De Ponti. *Wind Tunnel Data of Variable Skew Quad Plane*. 2023. DOI: https://doi.org/10.4121/21916509.v2.

[9] G. Hattenberger, B. Murat, and G. Michel. *Using the Paparazzi Uav System for Scientific Research*. IMAV conference and competition. 2014.

[10] B. Theys et al. *Wind tunnel testing of a VTOL MAV propeller in tilted operating mode*. 2014 ICUAS. 2014. DOI: 10.1109/icuas.2014.6842358.

[11] B. Theys et al. "Experimental and Numerical Study of MAV Propeller Performance in Oblique Flow". In: *Journal of aircraft* 3 (May 2017). DOI: 10.2514/1.c033618.

[12] C. Russel et al. *Wind Tunnel and Hover Performance Test Results for Multicopters cUAS Vehicles*. AHS 72nd Annual Forum. May 2016.